A Minimal Metabolic Model of Energy-Driven Dormancy in E. coli

George David Apostolidis[1*†], Aadreeta Biswas[1†] and Jeroen Mieras[1†]

[1*]Wageningen University and Research, Wageningen, The Netherlands.

[†]All authors contributed equally to this work.

1 Background

Growth–survival decisions in organisms ranging from microorganisms to human cells are regulated by cellular metabolism. This "low-energy" view of bacterial dormancy is supported by the conclusion of Himeoka & Mitarai [1] that the characteristic slow dynamics of persistence can be triggered solely by the depletion of high-energy cofactors, independently of genetic regulation. In this work, a rapid growth trajectory and a slow-timescale dormant trajectory were observed. A kinetic model of *E. coli* central carbon metabolism, explicitly incorporating the energy currency molecules ATP, ADP, and AMP, was developed for this purpose. Bacterial dormancy was demonstrated to originate from entirely non-genetic metabolic variations. Through the shift between high- and low-metabolic states, a universal regulatory principle is highlighted.

The phosphoenolpyruvate (PEP)–pyruvate (PYR)–oxaloacetate (OAA) node was examined in another study as a central metabolic switch point for carbon flux distribution in bacteria. At this metabolic node, ATP-dissipating futile cycles in which opposing reactions occur simultaneously can even be included in the in vivo flux. A tightly interconnected set of C3-carboxylation reactions (anaplerosis) and C4-decarboxylation reactions (gluconeogenesis) is operated there. A connection between catabolism, anabolism, and energy generation was made in an analysis by Sauer and Eikmanns [2].

Cellular decisions between rapid growth and reduced metabolic activity are consequently coupled to the metabolic state through the conserved signal of the ATP/ADP ratio. The regulatory logic observed in bacteria is mirrored by the shift toward a lower-energy, glycolysis-dependent state, in which energy charge not only reflects metabolic

activity but actively redirects fluxes through central nodes. Glycolytic flux is regulated by the cytosolic ATP/ADP ratio, with high ratios suppressing it and low ratios stimulating it, as highlighted by Maldonado and Lemasters [3]. The linkage between metabolic dynamics and broader principles of cellular physiology is thus established through the central role of the ATP/ADP ratio in determining whether cells operate in an energetically robust, growth-permissive state.

The principle that energy state determines how central nodes such as the PEP–PYR–OAA axis channel carbon is reflected in this behaviour. Carbon skeletons are redistributed away from oxidative metabolism toward biosynthetic or energy-balancing routes through the conversion of OAA to PEP by PEPCK. PEPCK is highlighted as functioning as a major cataplerotic valve that exports carbon from the TCA cycle into downstream pathways by Yang et al. [4]. A complementary study on how energy status reshapes metabolic fluxes is thus provided through the central role of PEPCK.

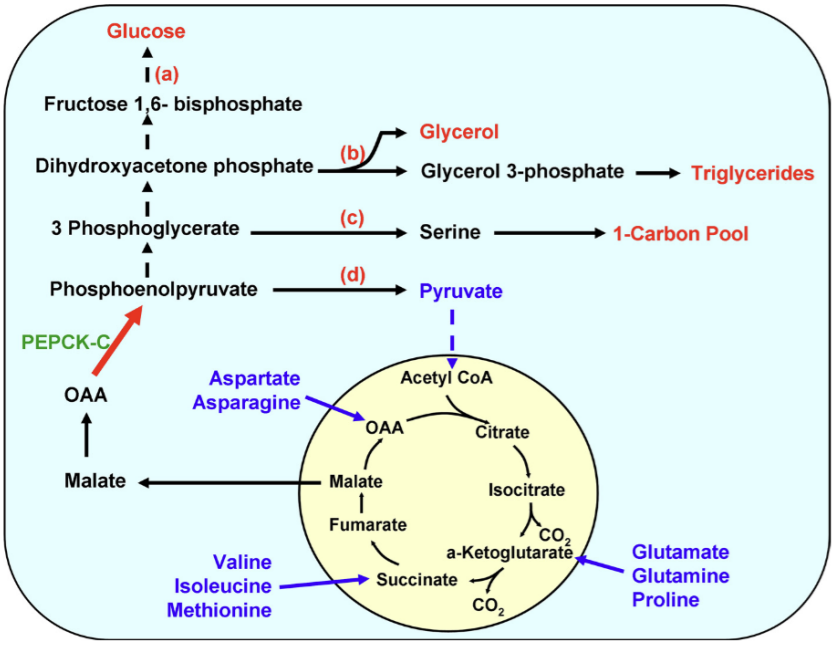

Fig. 1 Cataplerosis is shown in action as carbon is drawn from the TCA cycle by PEPCK, sending PEP into several downstream pathways and highlighting the central role of the PEP–OAA–PYR node.

The conditions under which transitions between dormant and growing states can be supported by a simplified metabolic model are the focus of this study. Reaction parameters are estimated using available time-series data, the system is reduced to two variables, and the resulting phase-plane behaviour is analysed across different energy states. It is hypothesised that both fast-growth and slow-relaxation trajectories can be generated within a reduced framework if the essential regulatory logic described above

is sufficient. Previous modelling efforts have been focused on large kinetic systems or on qualitative descriptions of carbon flux, leaving open the question of whether growth–dormancy transitions can be reproduced by a minimal system. Altogether, it is shown that flux through the PEP–PYR–OAA node is jointly regulated by energy charge and cataplerosis, forming the conceptual basis for our simplified model.

2 Methods

The degradation rate, denoted by d, is applied to all metabolites, and the values $r \in \{1,\, 0.1,\, 0.01\}$ are used to represent the experimental glucose uptake rates. The system was implemented through the following set of ordinary differential equations:

$$\frac{d[\mathrm{Glc}]}{dt} = -r\,\varphi\,\mathrm{Glc}, \tag{1}$$

$$\frac{d[\mathrm{PEP}]}{dt} = r\varphi\,\mathrm{Glc} + r\varphi\,\mathrm{OAA} + \varphi\,\mathrm{PYR} - (1+\varphi+d)\,\mathrm{PEP}, \tag{2}$$

$$\frac{d[\mathrm{PYR}]}{dt} = r\varphi\,\mathrm{OAA} + \varphi\,\mathrm{PEP} - (\varphi+d)\,\mathrm{PYR}, \tag{3}$$

$$\frac{d[\mathrm{OAA}]}{dt} = \mathrm{PEP} - \varphi\,\mathrm{OAA}. \tag{4}$$

Energy availability was represented by

$$\varphi = \max(1 - \mathrm{PYR}, \varphi_0),$$

where φ_0 sets the baseline ATP/ADP ratio. A four-dimensional system describing glucose (Glc), phosphoenolpyruvate (PEP), pyruvate (PYR), and oxaloacetate (OAA) was obtained by writing ODEs directly from the reaction scheme provided in the project description. All analyses were developed in Python (Version 3.12.12; 2025). A model of metabolism was then developed, parameterised, and analysed by building on the regulatory principles introduced in the Background.

For each parameter set p, simulations of the full ODE model were carried out for all three glucose uptake conditions. A total of 2,000 parameter sets covering the search intervals of d, φ_0, and OAA(0) were generated through Latin Hypercube Sampling. This provided the first stage of the parameter estimation strategy.

The system was then simulated over $t \in [0, 10]$ h using `solve_ivp` with absolute and relative tolerances of 10^{-8}. The baseline energy level φ_0 was restricted to the range $[0, 1]$. The degradation rate was assumed to be between 10^{-9} and 10^{-6} h^{-1}, following the project description and the expectation of slow metabolite turnover. Because OAA was not measured experimentally, its initial value OAA(0) was estimated within $[0, 10]$ mM. Initial PEP and PYR concentrations were taken directly from the experimental measurements at $t = 0$ for each value of r. The glucose concentration was set to $\mathrm{Glc}(0) = 1$ mM.

The reduced system was obtained by applying a quasi–steady-state approximation to OAA and by treating the glucose concentration as negligible after its initial rapid

decline driven by the $-r\varphi\,\mathrm{Glc}$ term. This led to a two-variable description of the qualitative dynamics of the central PEP–PYR node:

$$\frac{d\,\mathrm{PEP}}{dt} = f(\mathrm{PEP},\mathrm{PYR};p) \;=\; r\,\mathrm{PEP} + \varphi\,\mathrm{PYR} - (1+\varphi+d)\,\mathrm{PEP}, \tag{5}$$

$$\frac{d\,\mathrm{PYR}}{dt} = g(\mathrm{PEP},\mathrm{PYR};p) \;=\; (r+\varphi)\,\mathrm{PEP} - (\varphi+d)\,\mathrm{PYR}. \tag{6}$$

A fine parameter grid was then evaluated using the same scoring function. Twenty evenly spaced values were selected for each parameter within tightened bounds: ± 1 for $\mathrm{OAA}(0)$, ± 0.3 for $\log_{10}(d)$, and ± 0.1 for φ_0, while keeping the original constraints. This formed the second stage of the optimisation procedure. The parameter set with the lowest score from the LHS stage was used as the centre of this refined search.

The scoring function used to quantify model accuracy was

$$\Omega(p) = \sum_{i\in\{0.01,0.1,1\}} \sum_{j\in\{\mathrm{PEP},\mathrm{PYR}\}} \omega_{i,j}(p), \tag{7}$$

$$\omega_{i,j}(p) = \sum_{t=t_0}^{t_f} \frac{(D_{i,j}(t) - M_{i,j}(t;p))^2}{\sigma_{i,j}(t)^2}, \tag{8}$$

where the experimental data are denoted by $D_{i,j}(t)$, the model outputs by $M_{i,j}(t;p)$, and their standard deviations by $\sigma_{i,j}(t)$.

In the first optimisation stage, the full set of ODEs was simulated across all three glucose uptake conditions for each of the 2,000 parameter samples generated by Latin Hypercube Sampling. The sampling covered the search intervals of d, φ_0, and $\mathrm{OAA}(0)$.

To study the dynamics of the reduced system, phase-plane plots were generated using initial conditions

$$\mathrm{PEP}(0),\ \mathrm{PYR}(0) \in [0,2]\ \mathrm{mM}.$$

Nullclines were computed by solving $f = 0$ and $g = 0$ numerically across a dense grid. The Jacobian matrix was derived symbolically and its eigenvalues evaluated at candidate fixed points. Energy availability was varied across three regimes:

$$\varphi = \varphi_0, \qquad \varphi = 1 - \mathrm{PYR}, \qquad \varphi_0 \in [0, 0.05].$$

We adopted a Michaelis–Menten–type expression because, mathematically, it responds smoothly to small changes in PEP while preventing unrealistically sharp increases in φ. A simple linear function would cause φ to rise too quickly with PEP, which is not biologically plausible. To examine whether a switch out of dormancy could occur at low energy availability, we therefore introduced the modified feedback form

$$\varphi(P) = \varphi_0 + \alpha\,\frac{P}{K+P}.$$

Here α determines how strongly PEP improves the energy status, while K defines the PEP concentration required for half-maximal enhancement. When K is small, φ can

increase even at low PEP, making bistability more likely; when K is large, feedback is weaker and activation of growth requires higher PEP levels. This modification reflects realistic metabolic regulation in which the accumulation of glycolytic intermediates enhances ATP production.

The modified system was simulated from both dormant and perturbed initial conditions under the same low-energy baseline to assess whether positive feedback could enable escape from the dormant state.

All figures can be reproduced by running `core_metabollism_final.py` together with the files `core_metabolism_r001.csv`, `core_metabolism_r01.csv`, and `core_metabolism_r1.csv`. All code for model construction, parameter optimisation, and simulations is included in the accompanying `codes.zip` folder.

3 Results

A well-defined and physiologically meaningful region of parameter space was identified by the coarse LHS scan, providing the basis for the later fine-grid optimisation. The estimated baseline energy level φ_0 agrees with typical ATP/ADP ratios in non-starved *E. coli*, and the very small degradation rate d is consistent with the high stability of central carbon metabolites. All three inferred parameters therefore fall within biologically reasonable limits.

The best-performing parameter set from the coarse LHS search achieved a score of 4.00×10^5 and was given by

$$\mathrm{OAA}(0) = 1.11\,\mathrm{mM}, \qquad d = 1.61 \times 10^{-9}\,\mathrm{h}^{-1}, \qquad \varphi_0 = 0.132.$$

The score progression showed rapid improvement within the first 200 sampled parameter sets, after which the minimum score stabilised, indicating that the global search had converged.

Each of the 2,000 sampled parameter sets was evaluated by a weighted least-squares score that reduced the influence of time points with high measurement uncertainty. This score compared simulated and experimental PEP and PYR values across all three growth conditions ($r = 1$, 0.1, 0.01). These evaluations formed the coarse parameter search, which used Latin Hypercube Sampling across biologically plausible ranges for OAA(0), d, and φ_0. The global qualitative patterns of the experimental data are captured by the fitted parameter set, although some finer dynamical details differ between the simulations and the measurements. Persistent declines in PEP and PYR are predicted by the model for the lower glucose uptake rates ($r = 0.1$ and $r = 0.01$), with no late recovery. These unstable trajectories agree with earlier reports of reduced metabolic activity under nutrient limitation.

For the growth condition $r = 1$, the simulated trajectories shown in Figure 2 display an initial decrease in PEP followed by a rise, while PYR shows a gradual increase after a brief early drop. These trends match the qualitative behaviour observed experimentally, and the simulated curves follow most of the mean values reasonably well. These simulations were generated using the optimal parameter set identified by the scoring function.

A well-defined and physiologically meaningful region of parameter space was located by the coarse LHS search, providing a sound basis for the subsequent fine-grid optimisation. The estimated baseline energy level φ_0 agrees with expected ATP/ADP ratios in non-starved *E. coli*, and the very small degradation rate d is consistent with the high stability of central carbon metabolites. All three inferred parameters therefore fall within biologically reasonable ranges.

The internal organisation of the reduced model is altered by nutrient limitation, even though a well-defined phase-plane structure is retained under all conditions. Systematic shifts in the placement, curvature, and relative orientation of the nullclines occur as r decreases, and the vector fields show progressively slower and more restricted motion in low-glucose environments.

When the growth rate is reduced to $r = 0.01$, both nullclines are shifted toward lower PEP and PYR values, and their intersection moves toward the lower-left region of the state space. The flow field becomes more horizontal, and trajectories advance more slowly in the PYR direction. These changes indicate that strong nutrient limitation compresses the dynamics into a smaller range of feasible metabolite concentrations and produces a slower approach to equilibrium.

At the intermediate rate $r = 0.1$, a noticeable change in the phase-plane structure is observed: the PEP nullcline moves rightward, and the PYR nullcline becomes less steep near the intersection. This produces a more elongated flow pattern, with trajectories reaching the steady state more slowly and from fewer directions. The vertical components of the vector field weaken, reflecting reduced sensitivity of PYR to PEP at this nutrient level.

For $r = 1$, the nullclines intersect within a region where the vector field shows strong directional alignment, indicating rapid movement toward the steady state. The PEP nullcline has a broad slope, and the PYR nullcline curves upward with increasing PEP, creating a wide basin of attraction in the upper part of the phase plane.

The nullclines and vector fields for the three glucose uptake rates ($r = 1$, 0.1, 0.01) are shown in Figure 3. Each subplot displays how the two nullclines and the local flow field change as nutrient availability decreases. The phase planes were examined to characterise how the reduced PEP–PYR dynamics respond to different levels of glucose supply.

Once energy availability is set to a low value, all trajectories are predicted to collapse into a dormant state, regardless of the initial metabolic perturbation. A transition between dormant and growing states is not supported by the reduced formulation, and coexistence of distinct metabolic behaviours is not produced. These results indicate that the simplified two-equation model lacks the dynamical structure needed to generate recovery from dormancy.

A single low-PEP equilibrium is reached from all initial conditions, as shown in Figure 4. No rise in PEP or movement toward a more active state is observed. Instead, each simulated trajectory decays monotonically into the dormant configuration. This steady behaviour suggests that the reduced system possesses only one globally attracting equilibrium when the energy level is low.

The system was simulated under low-energy conditions by fixing $\varphi_0 = 0.05$. Four different initial metabolite states were selected to represent deeply dormant, moderately active, and perturbed conditions. These simulations were used to assess whether the reduced PEP–PYR model can reproduce recovery from dormancy.

4 Discussion

When estimating the parameter values, 2,000 different parameter sets were tested and optimisation was implemented based on the best scoring values. However, it is possible that a local optimum was selected instead of another combination of untested but lower-scoring values. Consequently, there may be other parameter sets that fit the data better and could potentially lead to improved results of the simplified model. This limitation should be kept in mind when interpreting the downstream analyses, since the reduced model is sensitive to the parameter regime in which it is evaluated.

A second important consideration concerns the quasi–steady-state assumption applied to OAA. The approximation assumes that OAA changes and reaches a steady state much faster than the other variables in the system, giving

$$\mathrm{OAA}_{\mathrm{QSS}} = \frac{\mathrm{PEP}}{\varphi}.$$

if we set the derivative of OAA to 0. However, the assumption is only valid for certain values of φ, because the relaxation time depends directly on φ. Since φ is never smaller than φ_0, the slowest possible relaxation occurs for $\varphi = \varphi_0$. As a result, the relaxation time is bounded above by $1/\varphi_0$, and OAA can only reach its steady state rapidly if φ_0 is not small. Examining the ODEs and the relaxation times for PEP and PYR shows that when φ_0 is low, OAA relaxes on a similar timescale as PEP and PYR. In such cases, no clear timescale separation exists, and the quasi–steady-state assumption is violated. This affects the reliability of removing OAA from the reduced model.

The differences between the three glucose uptake conditions ($r = 1$, 0.1, 0.01) further illustrate how sensitive the system is to metabolic context. Higher r values show faster PEP and PYR dynamics, whereas the lowest condition leads to much slower trajectories. These differences demonstrate how dependent the carbon flux is on nutrient availability. Fitting all datasets simultaneously constrained the parameters effectively, as any candidate solution needed to reproduce dynamics that varied by more than an order of magnitude in speed. This is relevant for the validity of the reduced model because any simplifications must still capture this broad range of behaviour.

The investigation also explored how PEP, PYR, and OAA behave when energy levels are low. The cells exhibit only two behaviours: one that leads to a dormant state and another that supports growth. We examined how to create a mechanism that could switch between these states to prevent dormancy under low-energy conditions. Upon analysing the initial data provided, we observed only one steady state and found no evidence of bistability. As we delved deeper, we attempted to adjust the model using values for α and K, yet both initial conditions converged to the same low-PEP steady state. Regardless of the combinations tested, we did not observe any change in the long-term behaviour of the system.

This behaviour mirrors the well-known ability of *E. coli* to enter metabolically inactive states under nutrient-poor or stressful conditions, where growth and biosynthesis are strongly suppressed. Because many antibiotics require active metabolism to exert their effect, these dormant states would be expected to confer increased tolerance; therefore, the model supports the idea that energy depletion can promote antibiotic persistence. The results indicate that the two equations selected, along with the reaction structure, demonstrate monostable behaviour, and that even after introducing feedback, no significant changes occur at low φ. To achieve a different outcome, we suggest reintroducing additional metabolic variables such as OAA or incorporating more complex regulatory interactions, as described in our first reference, rather than treating them as constants.

Finally, when examining the effect of r, we observed that increasing the scaling factor led to improved predictions regarding the behaviour of the system at lower energy levels. This indicates that the system cannot escape low-energy conditions spontaneously without external nutrient influx, because PEP and PYR enter the system with a rate positively correlated with r. The higher values imply that there is a necessary energetic threshold for the transition from the lag phase to exponential growth. This suggests that cells undergoing a lag phase must restore ATP levels and reactivate central carbon metabolism before growth becomes self-sustaining. In this study, we examined three scaling factors ($r = 1, 0.1, 0.01$), and further work could explore how cells respond to a wider range of values or values closer to 1, as these conditions produced more favourable outcomes.

Attributions

A collective contribution is reflected in the final project, as all discussions, decisions, analyses, and refinements were carried out jointly. A substantial role in the interpretation of results and in forming the biological conclusions was taken by Jeroen Mieras, who also contributed to the literature review and to discussions that guided the project. A major role in analysing and synthesising relevant literature, especially for the second and third research questions, was taken by Aadreeta Biswas, who also contributed to the biological interpretation of the modelling results. Primary responsibility for the coding aspects of the project—including refinement of the simulation framework, parameter fitting, and figure generation—was taken by George David Apostolidis, who also led the writing and assembly of the manuscript and organised the document.

An equal contribution across all components of the work was consistently aimed for by the group, and no major task relied solely on a single individual. The project was carried out collaboratively, with every component receiving input from all authors.

During the preparation of this work, the authors used ChatGPT 5.1 and Gemini 3, accessed through their respective online interfaces, to assist with clarifying mathematical steps, interpreting model behaviour, and improving the clarity of written sections. All AI-generated outputs were subsequently reviewed, revised, and edited by the authors, who take full responsibility for the final content of this report. Instances

in which these tools supported mathematical reasoning or data interpretation are explicitly indicated in the text.

References

[1] Y, H., N, M.: Emergence of growth and dormancy from a kinetic model of the escherichia coli central carbon metabolism. Physical Review Research **4**, 043223 (2022) https://doi.org/10.1103/PhysRevResearch.4.043223

[2] U, S., BJ, E.: The pep–pyruvate–oxaloacetate node as the switch point for carbon flux distribution in bacteria. FEMS Microbiology Reviews **29**, 765–794 (2005) https://doi.org/10.1016/j.femsre.2004.11.002

[3] EN, M., JJ, L.: Atp/adp ratio: the missed connection between mitochondria and the warburg effect. Mitochondrion **19**, 78–84 (2014) https://doi.org/10.1016/j.mito.2014.09.002

[4] J., Y., C., K.S., W., H.R.: What is the metabolic role of phosphoenolpyruvate carboxykinase? Journal of Biological Chemistry **284**(40), 27025–27029 (2009) https://doi.org/10.1074/jbc.R109.040543

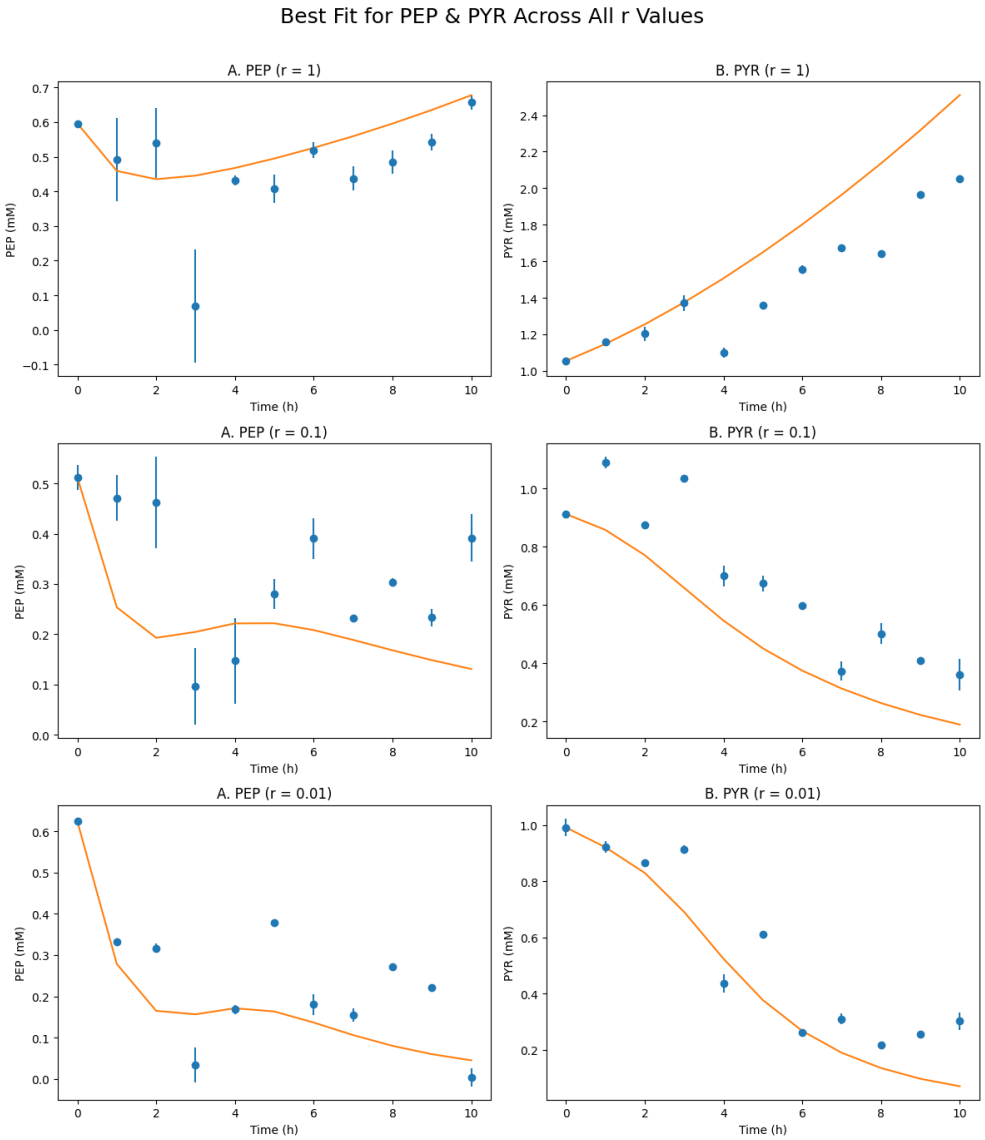

Fig. 2 The main features of the experimental trends are reflected by the model output: recovery is reproduced only for $r = 1$, while monotonic declines appear at lower uptake rates, despite some mismatches in the intermediate conditions.

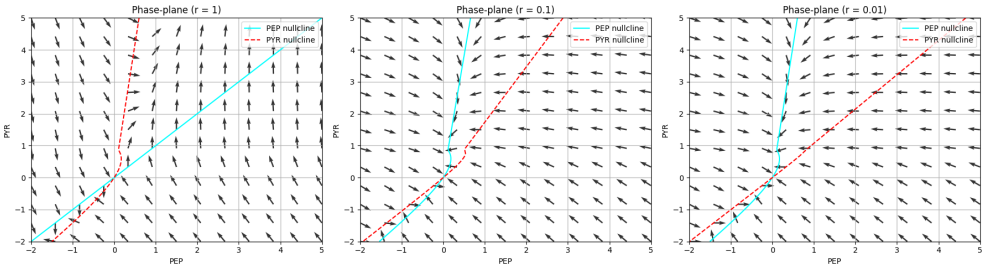

Fig. 3 Slower and more constrained dynamics under nutrient limitation are indicated by the phase planes, where decreasing r shifts both nullclines toward lower metabolite levels and produces more horizontal vector fields.

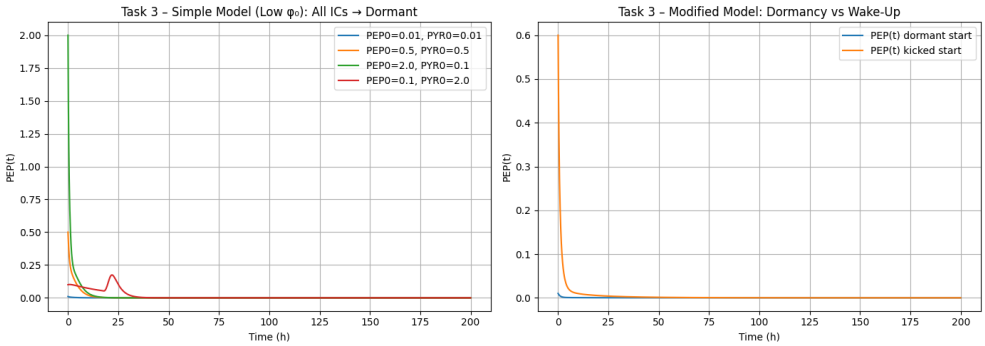

Fig. 4 Recovery from dormancy is not produced by either formulation of the reduced model, as all simulated trajectories collapse to the same low-PEP equilibrium under low-energy conditions.